PHYSICAL REVIEW D **96,** 095032 (2017)

Right-handed neutrino dark matter in the classically conformal U(1)′ extended standard model

Satsuki Oda,[1,2,*] Nobuchika Okada,[3,†] and Dai-suke Takahashi[1,2,‡]

[1]*Okinawa Institute of Science and Technology Graduate University (OIST), Onna, Okinawa 904-0495, Japan*

[2]*Research Institute, Meio University, Nago, Okinawa 905-8585, Japan*

[3]*Department of Physics and Astronomy, University of Alabama, Tuscaloosa, Alabama 35487, USA*

(Received 18 April 2017; revised manuscript received 20 August 2017; published 29 November 2017)

We consider the dark matter (DM) scenario in the context of the classically conformal U(1)′ extended standard model (SM), with three right-handed neutrinos (RHNs) and the U(1)′ Higgs field. The model is free from all of the U(1)′ gauge and gravitational anomalies in the presence of the three RHNs. We introduce a Z_2 parity in the model, under which an odd parity is assigned to one RHN, while all of the other particles are assigned to be Z_2 even, and hence the Z_2-odd RHN serves as a DM candidate. In this model, the U(1)′ gauge symmetry is radiatively broken through the Coleman-Weinberg mechanism, by which the electroweak symmetry breaking is triggered. There are three free parameters in our model—the U(1)′ charge of the SM Higgs doublet (x_H), the new U(1)′ gauge coupling (g_X), and the U(1)′ gauge boson (Z') mass ($m_{Z'}$)—which are severely constrained in order to solve the electroweak vacuum instability problem, and satisfy the LHC Run-2 bounds from the search for the Z' boson resonance. In addition to these constraints, we investigate the RHN DM physics. Because of the nature of classical conformality, we find that a RHN DM pair mainly annihilates into the SM particles through Z' boson exchange. This is the so-called Z'-portal DM scenario. Combining the electroweak vacuum stability condition, the LHC Run-2 bounds, and the cosmological constraint from the observed DM relic density, we find that all constraints work together to narrow the allowed parameter regions and, in particular, exclude $m_{Z'} \lesssim 3.5$ TeV. For the obtained allowed regions, we calculate the spin-independent cross section of the RHN DM with nucleons. We find that the resultant cross section is well below the current experimental upper bounds.

DOI: 10.1103/PhysRevD.96.095032

I. INTRODUCTION

There are important missing pieces in the Standard Model (SM), such as a candidate for dark matter (DM) and the tiny neutrino masses and their flavor mixings. The SM should be extended so as to supplement these missing pieces. The so-called seesaw mechanism is a natural way to reproduce the tiny neutrino masses [1–5], where heavy Majorana right-handed neutrinos (RHNs) are introduced. The minimal gauged $B-L$ model [6–11] is one of the simplest extensions of the SM with an extra gauge symmetry, in which the accidentally anomaly-free global $B-L$ (baryon number minus lepton number) in the SM is gauged. Three RHNs play an essential roll to cancel the gauge and gravitational anomalies of the model. Associated with the $B-L$ symmetry breaking, the RHNs acquire their Majorana masses, and hence the seesaw mechanism is automatically implemented. The minimal $B-L$ model can be generalized to the so-called minimal U(1)′ model [12]. Here, the U(1)′ gauge group is defined as a linear combination of the $U(1)_{B-L}$ and SM $U(1)_Y$ gauge groups, so that the U(1)′ model is anomaly-free.

In our previous work [13,14] we investigated the minimal U(1)′ model with classically conformal invariance.[1] In this model, the U(1)′ gauge symmetry is radiatively broken through the Coleman-Weinberg (CW) mechanism [53]. Given a negative mixing quartic coupling between the SM Higgs and U(1)′ Higgs fields, once the U(1)′ Higgs field develops a vacuum expectation value (VEV), a negative mass-squared of the SM Higgs doublet is generated, and thus the electroweak symmetry breaking is naturally triggered. In this model context, we investigated the electroweak vacuum instability problem in the SM. Employing the renormalization group (RG) equations at the two-loop level and the central values for the world average masses of the top quark ($m_t = 173.34$ GeV [54]) and the Higgs boson ($m_h = 125.09$ GeV [55]), we performed parameter scans to identify the parameter region that resolves the electroweak vacuum instability problem. We also investigated the ATLAS and CMS search limits at the LHC Run-2 (2015) for the U(1)′ gauge boson (Z') [56,57], and identified the allowed parameter regions in our model. Combining the

*satsuki.oda@oist.jp
†okadan@ua.edu
‡daisuke.takahashi@oist.jp

[1]See Refs. [15–52] for recent work on new physics models with classically conformal invariance.

constraints from electroweak vacuum stability and the LHC Run-2 results, we found a lower bound on the Z' boson mass. We also calculated self-energy corrections to the SM Higgs doublet field through the heavy states, the right-handed neutrinos, and the Z' boson, and found the naturalness bound as $m_{Z'} \lesssim 6$ TeV, in order to reproduce the right electroweak scale for a fine-tuning level better than 10%.

The so-called weakly interacting massive particle (WIMP) is one of the most promising candidates for DM, as it is in thermal equilibrium in the early Universe. Among many possibilities, a simple way to introduce WIMP DM in the minimal $U(1)'$ model was proposed in Ref. [58] (see also Ref. [59]), where Z_2 parity is introduced and an odd parity is assigned to one RHN, while all the other particles are assigned to be Z_2 even. We adapt this scheme in our minimal $U(1)'$ model with the classically conformal invariance, and the Z_2-odd RHN is a DM candidate, while the other two RHNs are utilized for the seesaw mechanism. Note that only two RHNs are sufficient to reproduce the neutrino oscillation data and the observed baryon asymmetry of the Universe through leptogenesis [60]. This system is called the minimal seesaw [61,62]. In our model, there are two ways for the RHN DM to interact with the SM particles. One is mediated by the Z' boson (Z' portal), and the other is mediated by the two Higgs bosons (Higgs portal) which are two mass eigenstates consisting of the SM Higgs and the $U(1)'$ Higgs bosons. Recently, the Z'-portal DM scenarios [63–91] have been intensively investigated, and the Higgs portal RHN DM scenarios [58,92,93] have been analyzed in detail.

In this paper, we consider the classically conformal $U(1)'$ extended SM with the RHN DM. As we mentioned above, the allowed parameter regions in the classically conformal model are severely constrained in order to solve the electroweak vacuum instability problem, and to satisfy the LHC limits from the search for the Z' boson resonance. In addition to these constraints, we will investigate the RHN DM physics. Because of the nature of classical conformality, we find that the mass mixing between the SM Higgs and the $U(1)'$ Higgs bosons is very small, so that the RHN DM pair annihilation process mediated by the Higgs bosons is highly suppressed. Therefore, we focus on the study of the Z'-portal RHN DM [80,89], and identify allowed parameter regions that reproduce the observed DM relic density from the Planck 2015 result [94]. We will show that the DM physics, LHC phenomenology, and the electroweak vacuum stability condition work together to narrow the allowed parameter regions. For the identified allowed regions, we also calculate the spin-independent cross section of the RHN DM with nucleons and compare our results with the current upper bounds from the direct DM search experiments.

This paper is organized as follows. In the next section, we introduce the classically conformal $U(1)'$ extended SM with Z'-portal RHN DM. We briefly review our previous work on the classically conformal $U(1)'$ model [13,14]. In Sec. III, we calculate the relic density of the Z'-portal RHN DM. In Sec. IV, we study the Z' boson production at the LHC Run-2 (2016) [95,96], and obtain the constraints on the model parameter space from the search results for the Z' boson resonance by the ATLAS and CMS collaborations. In Sec. V, we combine all of the results from the previous sections and narrow the allowed regions. In Sec. VI, we calculate the spin-independent cross section of the RHN DM with nucleons for the allowed parameter regions. The last section is devoted to conclusions.

II. THE CLASSICALLY CONFORMAL U(1)′ EXTENDED SM WITH RHN DM

In this section we briefly review the results of Ref. [14]. Although the model is extended to incorporate the RHN DM, the results presented here are essentially the same as those in Ref. [14].

A. The model

The model we will investigate is the anomaly-free $U(1)'$ extension of the SM with the classically conformal invariance, which is based on the gauge group $SU(3)_C \times SU(2)_L \times U(1)_Y \times U(1)'$. The particle contents of the model are listed in Table I. In addition to the SM particle content, three generations of RHNs ν_R^i and a $U(1)'$ Higgs field Φ are introduced. We also introduce the Z_2 parity [58], and assign an odd parity to one RHN ν_R^3, while the other particles, including ν_R^1 and ν_R^2, have even parity. The conservation of Z_2 parity ensures the stability of ν_R^3, which is a unique candidate for DM in our model.

The covariant derivative, which is relevant to $U(1)_Y \times U(1)'$, is defined as

TABLE I. Particle contents of the $U(1)'$ extended SM with Z_2 parity. In addition to the SM particle contents, three generations of RHNs ν_R^i ($i = 1, 2, 3$ denotes the generation index) and the $U(1)'$ Higgs field Φ are introduced. Under Z_2 parity, only one RHN ν_R^3 is odd, while the other particles, including ν_R^1 and ν_R^2, are even.

	$SU(3)_c$	$SU(2)_L$	$U(1)_Y$	$U(1)'$			Z_2
q_L^i	**3**	**2**	$+1/6$	x_q	$=$	$\frac{1}{3}x_H + \frac{1}{6}x_\Phi$	$+$
u_R^i	**3**	**1**	$+2/3$	x_u	$=$	$\frac{4}{3}x_H + \frac{1}{6}x_\Phi$	$+$
d_R^i	**3**	**1**	$-1/3$	x_d	$=$	$-\frac{2}{3}x_H + \frac{1}{6}x_\Phi$	$+$
ℓ_L^i	**1**	**2**	$-1/2$	x_ℓ	$=$	$-x_H - \frac{1}{2}x_\Phi$	$+$
$\nu_R^{1,2}$	**1**	**1**	0	x_ν	$=$	$-\frac{1}{2}x_\Phi$	$+$
ν_R^3	**1**	**1**	0	x_ν	$=$	$-\frac{1}{2}x_\Phi$	$-$
e_R^i	**1**	**1**	-1	x_e	$=$	$-2x_H - \frac{1}{2}x_\Phi$	$+$
H	**1**	**2**	$+1/2$	x_H	$=$	x_H	$+$
Φ	**1**	**1**	0	x_Φ	$=$	x_Φ	$+$

$$D_\mu \equiv \partial_\mu - i\begin{pmatrix} Y_1 & Y_X \end{pmatrix}\begin{pmatrix} g_1 & g_{1X} \\ g_{X1} & g_X \end{pmatrix}\begin{pmatrix} B_\mu \\ B'_\mu \end{pmatrix}, \quad (2.1)$$

where Y_1 (Y_X) is the $\mathrm{U}(1)_Y$ [$U(1)'$] charge of a particle, and the gauge couplings g_{X1} and g_{1X} are associated with the kinetic mixing between the two U(1) gauge bosons. In order to reproduce the observed fermion masses and flavor mixings, we introduce the following Yukawa interactions:

$$\begin{aligned}\mathcal{L}_{\mathrm{Yukawa}} = &-\sum_{i=1}^{3}\sum_{j=1}^{3} Y_u^{ij}\overline{q_L^i}\,\tilde{H}\,u_R^j - \sum_{i=1}^{3}\sum_{j=1}^{3} Y_d^{ij}\overline{q_L^i}H d_R^j \\ &-\sum_{i=1}^{3}\sum_{j=1}^{3} Y_e^{ij}\overline{\ell_L^i}H e_R^j - \sum_{i=1}^{3}\sum_{j=1}^{2} Y_\nu^{ij}\overline{\ell_L^i}\,\tilde{H}\,\nu_R^j \\ &-\sum_{i=1}^{3} Y_M^i \Phi\overline{\nu_R^{ic}}\nu_R^i + \mathrm{H.c.}, \end{aligned} \quad (2.2)$$

where $\tilde{H} \equiv i\tau^2 H^*$, and the fourth and fifth terms on the right-hand side allow the seesaw mechanism to generate neutrino masses. Without loss of generality, the Majorana Yukawa couplings in the fifth term are already diagonalized in our basis. Because of the Z_2 parity, only two generations of RHNs are involved in the neutrino Dirac Yukawa couplings and hence the neutrino Dirac mass matrix is 2×3. Once the $\mathrm{U}(1)'$ Higgs field Φ develops a VEV, the $\mathrm{U}(1)'$ symmetry is broken and the Majorana mass terms for the RHNs are generated. After the electroweak symmetry breaking, the seesaw mechanism [1–5] is automatically implemented, except that only two generations of RHNs are relevant. This system is the minimal seesaw [61,62], which possesses a number of free parameters Y_ν^{ij} and Y_M^j ($i = 1, 2, 3$, $j = 1, 2$), enough to reproduce the neutrino oscillation data with a prediction of one massless eigenstate.

In the particle contents, the two parameters (x_H and x_Φ) reflect the fact that the $\mathrm{U}(1)'$ gauge group can be defined as a linear combination of the SM $\mathrm{U}(1)_Y$ and $\mathrm{U}(1)_{B-L}$ gauge groups. Since the $\mathrm{U}(1)'$ gauge coupling g_X is a free parameter of the model and it always appears as a product ($x_\Phi g_X$ or $x_H g_X$), we fix $x_\Phi = 2$ without loss of generality throughout this paper. This convention excludes the case that the $\mathrm{U}(1)'$ gauge group is identical to the SM $\mathrm{U}(1)_Y$. The choice of $(x_H, x_\Phi) = (0, 2)$ corresponds to the $\mathrm{U}(1)_{B-L}$ model. Another example is $(x_H, x_\Phi) = (-1, 2)$, which corresponds to the SM with the so-called $\mathrm{U}(1)_R$ symmetry. When we choose $(x_H, x_\Phi) = (-16/41, 2)$, the beta function of g_{X1} (g_{1X}) at the one-loop level only has terms proportional to g_{X1} (g_{1X}) [13]. This is the orthogonality condition between the $\mathrm{U}(1)_Y$ and $\mathrm{U}(1)'$ at the one-loop level, under which g_{X1} and g_{1X} do not evolve once we have set $g_{X1} = g_{1X} = 0$ at an energy scale.

Imposing the classically conformal invariance, the scalar potential is given by

$$V = \lambda_H (H^\dagger H)^2 + \lambda_\Phi (\Phi^\dagger \Phi)^2 + \lambda_{\mathrm{mix}} (H^\dagger H)(\Phi^\dagger \Phi), \quad (2.3)$$

where the mass terms are forbidden by the conformal invariance. If λ_{mix} is negligibly small, we can analyze the Higgs potential separately for Φ and H as a good approximation. This will be justified in the following subsections. When the Majorana Yukawa couplings Y_M^i are negligible compared to the $\mathrm{U}(1)'$ gauge coupling, the Φ sector is identical to the original CW model [53], and thus the radiative $\mathrm{U}(1)'$ symmetry breaking will be achieved. Once Φ develops a VEV through the CW mechanism, the tree-level mass term for the SM Higgs doublet is effectively generated through λ_{mix} in Eq. (2.3). Taking λ_{mix} negative, the induced mass-squared for the Higgs doublet is negative and, as a result, the electroweak symmetry breaking is driven in the same way as in the SM.

B. Radiative $\mathrm{U}(1)'$ gauge symmetry breaking

Assuming λ_{mix} is negligibly small, we first analyze the $\mathrm{U}(1)'$ Higgs sector. Without mass terms, the Coleman-Weinberg potential [53] at the one-loop level is found to be

$$V(\phi) = \frac{\lambda_\Phi}{4}\phi^4 + \frac{\beta_\Phi}{8}\phi^4\left(\ln\left[\frac{\phi^2}{v_\phi^2}\right] - \frac{25}{6}\right), \quad (2.4)$$

where $\phi/\sqrt{2} = \Re[\Phi]$, and we have chosen the renormalization scale to be the VEV of Φ ($\langle\phi\rangle = v_\phi$). Here, the coefficient of the one-loop quantum corrections is given by

$$\begin{aligned}\beta_\Phi &= \frac{1}{16\pi^2}\left[20\lambda_\Phi^2 + 6x_\Phi^4(g_{X1}^2 + g_X^2)^2 - 16\sum_i (Y_M^i)^4\right] \\ &\simeq \frac{1}{16\pi^2}\left[6(x_\Phi g_X)^4 - 16\sum_i (Y_M^i)^4\right], \end{aligned} \quad (2.5)$$

where in the last expression we have used $\lambda_\Phi^2 \ll (x_\Phi g_X)^4$ as usual in the CW mechanism and set $g_{X1} = g_{1X} = 0$ at $\langle\phi\rangle = v_\phi$ for simplicity. The stationary condition $dV/d\phi|_{\phi=v_\phi} = 0$ leads to

$$\lambda_\Phi = \frac{11}{6}\beta_\Phi, \quad (2.6)$$

and this λ_Φ is nothing but a renormalized self-coupling at v_ϕ defined as

$$\lambda_\Phi = \frac{1}{3!}\frac{d^4V(\phi)}{d\phi^4}\bigg|_{\phi=v_\phi}. \quad (2.7)$$

For a more detailed discussion, see Ref. [32].

Associated with this radiative $\mathrm{U}(1)'$ symmetry breaking (as well as the electroweak symmetry breaking), the $\mathrm{U}(1)'$ gauge boson (Z' boson), the Majorana RHNs $\nu_R^{1,2}$, and the RHN DM particle ν_R^3 acquire their masses as

$$m_{Z'} = \sqrt{(x_\Phi g_X v_\phi)^2 + (x_H g_X v_h)^2} \simeq x_\Phi g_X v_\phi,$$
$$m_{N^{1,2}} = \sqrt{2} Y_M^{1,2} v_\phi, \qquad m_{\rm DM} = \sqrt{2} Y_M^3 v_\phi, \tag{2.8}$$

where $v_h = 246$ GeV is the SM Higgs VEV, and we have used $x_\Phi v_\phi \gg x_H v_h$, which will be verified below. In this paper, we assume degenerate masses for $\nu_R^{1,2}$ ($Y_M^1 = Y_M^2 = y_M$, equivalently, $m_{N^{1,2}} = m_N$) for simplicity. The U(1)′ Higgs boson mass is given by

$$\begin{aligned} m_\phi^2 &= \left.\frac{d^2 V}{d\phi^2}\right|_{\phi = v_\phi} \\ &= \beta_\Phi v_\phi^2 \simeq \frac{1}{8\pi^2}(3(x_\Phi g_X)^4 - 16 y_M^4 - 8 y_{\rm DM}^4) v_\phi^2 \\ &\simeq \frac{1}{8\pi^2}\frac{3m_{Z'}^4 - 4m_N^4 - 2m_{\rm DM}^4}{v_\phi^2}, \end{aligned} \tag{2.9}$$

where $y_{\rm DM} = Y_M^3$. When the Yukawa couplings are negligibly small, this equation reduces to the well-known relation derived in the original paper by Coleman and Weinberg [53]. For a sizable Majorana mass, this formula indicates that the potential minimum disappears, so that there is an upper bound on the RHN mass for the U(1)′ symmetry to be broken radiatively. This is in fact the same reason why the CW mechanism in the SM Higgs sector fails to break the electroweak symmetry when the top Yukawa coupling is large (as observed). In order to avoid the destabilization of the U(1)′ Higgs potential, we simply set $m_{Z'}^4 \gg m_N^4$ in the following analysis, while $m_{\rm DM} \simeq m_{Z'}/2$, as we will find in the next section. Note that this condition does not mean that the Majorana RHNs must be very light, even a factor difference between $m_{Z'}$ and m_N is enough to satisfy the condition. For simplicity, we set $y_M = 0$ at v_ϕ in the following RG analysis as an approximation.

C. Electroweak symmetry breaking

Let us now consider the SM Higgs sector. In our model, the electroweak symmetry breaking is achieved in a very simple way. Once the U(1)′ symmetry is radiatively broken, the SM Higgs doublet mass is generated through the mixing quartic term between H and Φ in the scalar potential in Eq. (2.3),

$$V(h) = \frac{\lambda_H}{4} h^4 + \frac{\lambda_{\rm mix}}{4} v_\phi^2 h^2, \tag{2.10}$$

where we have replaced H by $H = 1/\sqrt{2}(0, h)$ in the unitary gauge. Choosing $\lambda_{\rm mix} < 0$, the electroweak symmetry is broken in the same way as in the SM [25,26]. However, we should note that a crucial difference from the SM is that, in our model, the electroweak symmetry breaking originates from the radiative breaking of the U(1)′ gauge symmetry. At the tree level, the stationary condition $V'|_{h=v_h} = 0$ leads to the relation $|\lambda_{\rm mix}| = 2\lambda_H (v_h/v_\phi)^2$, and the Higgs boson mass m_h is given by

$$m_h^2 = \left.\frac{d^2 V}{dh^2}\right|_{h=v_h} = |\lambda_{\rm mix}| v_\phi^2 = 2\lambda_H v_h^2. \tag{2.11}$$

In the following RG analysis, this is used as the boundary condition for $\lambda_{\rm mix}$ at the renormalization scale $\mu = v_\phi$. Note that since $\lambda_H \sim 0.1$ and $v_\phi \gtrsim 10$ TeV by the large electron-positron collider (LEP) constraint [97–99], $|\lambda_{\rm mix}| \lesssim 10^{-5}$, which is very small.

In our discussion about the U(1)′ symmetry breaking, we neglected $\lambda_{\rm mix}$ by assuming it to be negligibly small. Here we justify this treatment. In the presence of $\lambda_{\rm mix}$ and the Higgs VEV, Eq. (2.6) is modified as

$$\lambda_\Phi = \frac{11}{6}\beta_\Phi + \frac{|\lambda_{\rm mix}|}{2}\left(\frac{v_h}{v_\phi}\right)^2 \simeq \frac{1}{2v_\phi^4}\left(\frac{11}{8\pi^2} m_{Z'}^4 + m_h^2 v_h^2\right). \tag{2.12}$$

Considering the current LHC Run-2 bound from the search for Z' boson resonances [95,96], $m_{Z'} \gtrsim 4$ TeV, we find that the first term in the parentheses in the last equality is 5 orders of magnitude greater than the second term, and therefore we can analyze the two Higgs sectors separately.

D. Solving the electroweak vacuum instability

In the SM with the observed Higgs boson mass of $m_h = 125.09$ GeV [55], the RG evolution of the SM Higgs quartic coupling shows that the running coupling becomes negative at the intermediate scale $\mu \simeq 10^{10}$ GeV [100] for $m_t = 173.34$ GeV [54], and hence the electroweak vacuum is unstable. In our U(1)′ extended SM, however, there is a parameter region to solve this electroweak vacuum instability problem [13,14].[2] There are only three free parameters in our model, x_H, v_ϕ, and g_X, which are also interpreted as x_H, $m_{Z'}$, and $\alpha_{g_X} = g_X^2/(4\pi)$. The inputs of the couplings at v_ϕ are determined by these three parameters. In Fig. 1(a), we show the RG evolution of the SM Higgs quartic coupling in our model (solid line), along with the SM result (dashed line). Here, we have taken $x_H = -0.575$, $m_{Z'} = 4$ TeV, and $\alpha_{g_X} = 0.01$, which corresponds to $v_\phi = 5.64$ TeV and $g_X(v_\phi) = 0.354$, as an example. The Higgs quartic coupling remains positive all the way up to the Planck mass scale, so the electroweak vacuum instability problem is solved.

In order to identify a parameter region to resolve the electroweak vacuum instability, we perform parameter

[2] In the absence of the classical conformal invariance, the electroweak vacuum instability problem was investigated in Refs. [84,101–103].

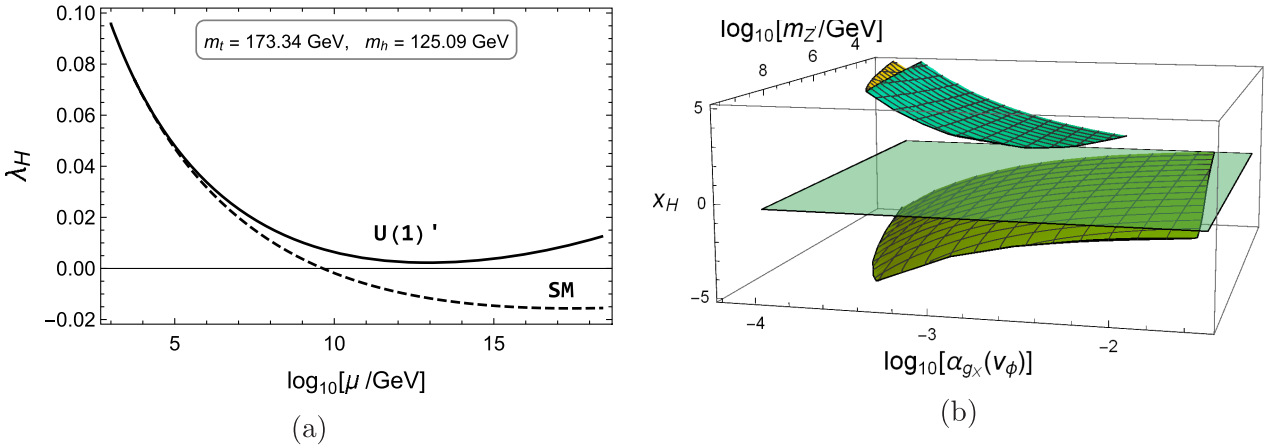

FIG. 1. (a) The evolutions of the Higgs quartic coupling λ_H (solid line) for the inputs $m_t = 173.34$ GeV and $m_h = 125.09$ GeV, along with the SM case (dashed line). Here, we have taken $x_H = -0.575$, $m_{Z'} = 4$ TeV. and $\alpha_{g_X} = 0.01$, which corresponds to $v_\phi = 5.64$ TeV and $g_X(v_\phi) = 0.354$. (b) The result of the three-dimensional parameter scans for v_ϕ, g_X, and x_H, shown in the ($m_{Z'}$/GeV, α_{g_X}, x_H) parameter space with $m_{Z'} \simeq x_\Phi g_X v_\phi$. As a reference, a horizontal plane for $x_H = -16/41$ is shown, which corresponds to the orthogonal case.

scans for the free parameters x_H, v_ϕ, and g_X. In this analysis, we impose several conditions on the running couplings at $v_\phi \le \mu \le M_P$ ($M_P = 2.44 \times 10^{18}$ GeV is the reduced Planck mass): the stability conditions of the Higgs potential (λ_H, $\lambda_\Phi > 0$), and the perturbative conditions that all the running couplings remain in the perturbative regime, namely, g_i^2 ($i = 1, 2, 3$), g_X^2, g_{X1}^2, $g_{1X}^2 < 4\pi$ and λ_H, λ_Φ, $\lambda_{\rm mix} < 4\pi$. For theoretical consistency, we also impose the condition that the two-loop beta functions are smaller than the one-loop beta functions (see Ref. [14] for details). In Fig. 1(b), we show the result of our parameter scans in the three-dimensional parameter space of $(m_{Z'}, \alpha_{g_X}, x_H)$. As a reference, we show a horizontal plane corresponding to the orthogonal case $x_H = -16/41$. There is no overlapping of the plane with the resultant parameter regions to resolve the electroweak vacuum instability.

E. Naturalness bounds from SM Higgs mass corrections

Once the classically conformal symmetry is radiatively broken by the CW mechanism, the masses for the Z' boson and the Majorana RHNs are generated, and they contribute to self-energy corrections of the SM Higgs doublet. If the U(1)$'$ gauge symmetry breaking scale is very large, the self-energy corrections may exceed the electroweak scale and require us to fine-tune the model parameters to reproduce the correct electroweak scale. See Ref. [104] for related discussions. As heavy states, we have the RHNs and Z' boson, whose masses are generated by the U(1)$'$ gauge symmetry breaking.

Since the original theory is classically conformal and defined as a massless theory, the self-energy corrections to the SM Higgs doublet originate from corrections to the mixing quartic coupling $\lambda_{\rm mix}$. Thus, what we calculate to derive the naturalness bounds are quantum corrections to the term $\lambda_{\rm mix} h^2\phi^2$ in the effective Higgs potential

$$V_{\rm eff} \supset \frac{\lambda_{\rm mix}}{4} h^2\phi^2 + \frac{\beta_{\lambda_{\rm mix}}}{8} h^2\phi^2(\ln[\phi^2] + C), \tag{2.13}$$

where the logarithmic divergence and the terms independent of ϕ are all encoded in C. Here, the major contributions to quantum corrections are from the Z' boson loops:

$$\beta_{\lambda_{\rm mix}} \supset \frac{12 x_H^2 x_\Phi^2 g_X^4}{16\pi^2} - \frac{4(19x_H^2 + 10 x_H x_\Phi + x_\Phi^2) x_\Phi^2 y_t^2 g_X^4}{(16\pi^2)^2}, \tag{2.14}$$

where the first term is from the one-loop diagram, and the second one is from the two-loop diagram [25,26] involving the Z' boson and the top quark. By adding a counterterm, we renormalize the coupling $\lambda_{\rm mix}$ with the renormalization condition,

$$\left.\frac{\partial^4 V_{\rm eff}}{\partial h^2 \partial \phi^2}\right|_{h=0,\phi=v_\phi} = \lambda_{\rm mix}, \tag{2.15}$$

where $\lambda_{\rm mix}$ is the renormalized coupling. As a result, we obtain

$$V_{\rm eff} \supset \frac{\lambda_{\rm mix}}{4} h^2\phi^2 + \frac{\beta_{\lambda_{\rm mix}}}{8} h^2\phi^2 \left(\ln\left[\frac{\phi^2}{v_\phi}\right] - 3\right). \tag{2.16}$$

Substituting $\phi = v_\phi$, we obtain the SM Higgs self-energy correction as

$$\Delta m_h^2 = -\frac{3}{4}\beta_{\lambda_{\rm mix}} v_\phi^2 \sim -\frac{9}{4\pi} x_H^2 \alpha_{g_X} m_{Z'}^2 + \frac{3m_t^2}{32\pi^3 v_h^2}(19x_H^2 + 20x_H + 4)\alpha_{g_X} m_{Z'}^2. \tag{2.17}$$

For the stability of the electroweak vacuum, we impose $\Delta m_h^2 \lesssim m_h^2$ as the naturalness bound. The most important contribution to Δm_h^2 is the first term of Eq. (2.17) generated through the one-loop diagram with the Z' gauge boson, and the second term becomes important in the case of the $U(1)_{B-L}$ model, where $x_H = 0$.

If Δm_h^2 is much larger than the electroweak scale, we need a fine-tuning of the tree-level Higgs mass ($|\lambda_{\rm mix}| v_\phi^2/2$) to reproduce the correct SM Higgs VEV, $v_h = 246$ GeV. We simply evaluate a fine-tuning level as

$$\delta = \frac{m_h^2}{2|\Delta m_h^2|}. \tag{2.18}$$

Here, $\delta = 0.1$, for example, indicates that we need to fine-tune the tree-level Higgs mass-squared at the 10% accuracy level.

III. RELIC DENSITY OF THE RHN DM

In this section, we calculate the thermal relic density of the RHN DM and identify the model parameter region to be consistent with the Planck 2015 measurement [94] (68% confidence level):

$$\Omega_{\rm DM} h^2 = 0.1198 \pm 0.0015. \tag{3.1}$$

In our model, the RHN DM particles mainly annihilate into the SM particles through the s-channel process mediated by the $U(1)'$ gauge boson Z'.

The Boltzmann equation of the RHN DM is given by

$$\frac{dY}{dx} = -\frac{xs\langle\sigma v\rangle}{H(m_{\rm DM})}(Y^2 - Y_{\rm EQ}^2), \tag{3.2}$$

where the temperature of the Universe is normalized by the mass of the RHN DM $x = m_{\rm DM}/T$, $H(m_{\rm DM})$ is the Hubble parameter at $T = m_{\rm DM}$, s is the entropy density, $Y = n/s$ is the yield of the RHN DM which is defined by the ratio of the number density n to s, $Y_{\rm EQ}$ is the yield in the thermal equilibrium, and $\langle\sigma v\rangle$ is the thermal-averaged product of the RHN DM annihilation cross section σ and relative velocity v. The explicit formulas for these are summarized as follows:

$$s = \frac{2\pi^2}{45} g_* \frac{m_{\rm DM}^3}{x^3}, \quad H(m_{\rm DM}) = \sqrt{\frac{\pi^2}{90} g_*}\frac{m_{\rm DM}^2}{M_{\rm P}}, \quad sY_{\rm EQ} = \frac{g_{\rm DM}}{2\pi^2}\frac{m_{\rm DM}^3}{x} K_2(x), \tag{3.3}$$

where $g_{\rm DM} = 2$ is the number of degrees of the freedom for the RHN DM, g_* is the effective total number of degrees of freedom for particles in thermal equilibrium (in this paper, we set $g_* = 106.75$ for the SM particles), and K_2 is the modified Bessel function of the second kind. The thermally averaged annihilation cross section times velocity is given by

$$\langle\sigma v\rangle = (sY_{\rm EQ})^{-2} g_{\rm DM}^2 \frac{m_{\rm DM}}{64\pi^4 x}\int_{4m_{\rm DM}^2}^{\infty} ds\hat{\sigma}(s)\sqrt{s}K_1\left(\frac{x\sqrt{s}}{m_{\rm DM}}\right), \tag{3.4}$$

where the reduced cross section is defined as $\hat{\sigma}(s) = 2(s - 4m_{\rm DM}^2)\sigma(s)$ with the total cross section $\sigma(s)$, and K_1 is the modified Bessel function of the first kind. The total cross section of the RHN DM annihilation process $\nu_R^3\nu_R^3 \to Z' \to f\bar{f}$ (f denotes the SM fermion)[3] is calculated as

$$\sigma(s) = \frac{\pi}{3}\alpha_{g_X}^2 \frac{\sqrt{s(s-4m_{\rm DM}^2)}}{(s-m_{Z'}^2)^2 + m_{Z'}^2\Gamma_{Z'}^2} \times \left[\frac{103x_H^2 + 86x_H + 37}{3} + \frac{17x_H^2 + 10x_H + 2 + (7x_H^2 + 20x_H + 4)\frac{m_t^2}{s}}{3} \times \sqrt{1 - \frac{4m_t^2}{s}} + 18x_H^2 \frac{(s-m_{Z'}^2)^2}{s(s-4m_{\rm DM}^2)}\frac{m_{\rm DM}^2 m_t^2}{m_{Z'}^4}\sqrt{1-\frac{4m_t^2}{s}}\right], \tag{3.5}$$

where the total decay width of the Z' boson is given by

[3] Although there are also other annihilation processes, such as $\nu_R^3\nu_R^3 \to \phi\phi$, $\nu_R^3\nu_R^3 \to \phi Z'$ and $\nu_R^3\nu_R^3 \to Z'Z'$ (see, for example, Ref. [105]), all of these cross sections are estimated to be much less than 1 pb, which is a typical cross section to reproduce $\Omega_{\rm DM}h^2 \simeq 0.1$, for $\alpha_{g_X} \sim 0.01$ (see Figs. 5 and 6), $y_{\rm DM} \sim g_X$, and $m_{\rm DM} \sim 1$ TeV.

$$\Gamma_{Z'} = \frac{\alpha_{g_X} m_{Z'}}{6}\left[\frac{103x_H^2+86x_H+37}{3} + \frac{17x_H^2+10x_H+2+(7x_H^2+20x_H+4)\frac{m_t^2}{m_{Z'}^2}}{3}\sqrt{1-\frac{4m_t^2}{m_{Z'}^2}} + 2\left(1-\frac{4m_N^2}{m_{Z'}^2}\right)^{\frac{3}{2}}\theta\left(\frac{m_{Z'}^2}{m_N^2}-4\right) + \left(1-\frac{4m_{\rm DM}^2}{m_{Z'}^2}\right)^{\frac{3}{2}}\theta\left(\frac{m_{Z'}^2}{m_{\rm DM}^2}-4\right)\right]. \quad (3.6)$$

Here, we have neglected all SM fermion masses except for the top quark mass m_t.

By solving the Boltzmann equation (3.2) numerically, we find the asymptotic value of the yield $Y(\infty)$, and the present DM relic density is given by

$$\Omega_{\rm DM}h^2 = \frac{m_{\rm DM}s_0 Y(\infty)}{\rho_c/h^2}, \quad (3.7)$$

where $s_0 = 2890\ {\rm cm}^{-3}$ is the entropy density of the present Universe, and $\rho_c/h^2 = 1.05\times10^{-5}\ {\rm GeV/cm}^3$ is the critical density. Our analysis involves four parameters, namely, α_{g_X}, $m_{Z'}$, $m_{\rm DM}$, and x_H. In Fig. 2 we show the resultant RHN DM relic density as a function of the RHN DM mass $m_{\rm DM}$ for $m_{Z'} = 4$ TeV and $x_H = -0.575$, along with the range of the observed DM relic density, $0.1183 \le \Omega_{\rm DM}h^2 \le 0.1213$ [94] (two horizontal dashed lines). The solid lines from top to bottom show the resultant RHN DM relic densities for various values of the gauge coupling: $\alpha_{g_X} = 0.002$, 0.00235, 0.003, 0.004, and 0.005. The plots indicate the lower bound on $\alpha_{g_X} \ge 0.00235$ for $m_{Z'} = 4$ TeV and $x_H = -0.575$ in order to reproduce the observed relic density. In addition, we can see that the enhancement of the RHN DM annihilation cross section via the Z' boson resonance is necessary to satisfy the cosmological constraint, and hence $m_{\rm DM} \simeq m_{Z'}/2$.

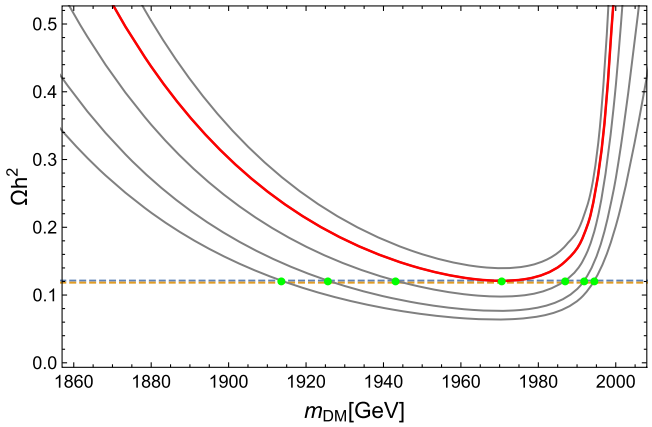

FIG. 2. The relic density of the RHN DM as a function of its mass ($m_{\rm DM}$). We have fixed $x_H = -0.575$ and $m_{Z'} = 4$ TeV, and show the relic densities for various values of the gauge coupling: $\alpha_{g_X} = 0.002$, 0.00235, 0.003, 0.004, and 0.005 (solid lines from top to bottom). The two horizontal lines denote the range of the observed DM relic density, $0.1183 \le \Omega_{\rm DM}h^2 \le 0.1213$ in the Planck 2015 results [94].

IV. COLLIDER CONSTRAINTS ON THE U(1)′ Z′ BOSON

The ATLAS and CMS collaborations have searched for the Z' boson resonance at the LHC Run-1 with $\sqrt{s} = 8$ TeV, and continued the search at the LHC Run-2 with $\sqrt{s} = 13$ TeV. The most stringent bounds on the Z' boson production cross section times branching ratio have been obtained by using the dilepton final state. For the so-called sequential SM Z' (Z'_{SSM}) model [106], where the Z'_{SSM} boson has exactly the same couplings with the SM fermions as those of the SM Z boson, the latest cross section bounds from the LHC Run-2 results lead to lower bounds on the Z'_{SSM} boson mass of $m_{Z'_{SSM}} \ge 4.05$ TeV in the ATLAS 2016 results [95] and $m_{Z'_{SSM}} \ge 4.0$ TeV in the CMS 2016 results [96], respectively. We interpret these ATLAS and CMS results in the U(1)′ Z' boson case and derive constraints on x_H, α_{g_X}, and $m_{Z'}$.

We calculate the dilepton production cross section for the process $pp \to Z' + X \to \ell^+\ell^- + X$. The differential cross section with respect to the invariant mass $M_{\ell\ell}$ of the final-state dilepton is described as

$$\frac{d\sigma}{dM_{\ell\ell}} = \sum_{a,b}\int_{\frac{M_{\ell\ell}^2}{E_{\rm CM}^2}}^1 dx_1 \frac{2M_{\ell\ell}}{x_1 E_{\rm CM}^2} f_a(x_1, M_{\ell\ell}^2) \times f_b\left(\frac{M_{\ell\ell}^2}{x_1 E_{\rm CM}^2}, M_{\ell\ell}^2\right)\hat{\sigma}(\bar{q}q \to Z' \to \ell^+\ell^-), \quad (4.1)$$

where f_a is the parton distribution function for a parton a, and $E_{\rm CM} = 13$ TeV is the center-of-mass energy of the LHC Run-2. In our numerical analysis, we employ CTEQ5M [107] for the parton distribution functions. In the case of the U(1)′ model, the cross sections for the colliding partons are given by

$$\hat{\sigma}(\bar{u}u \to Z' \to \ell^+\ell^-) = \frac{\pi\alpha_{g_X}^2}{81}\frac{M_{\ell\ell}^2}{(M_{\ell\ell}^2 - m_{Z'}^2)^2 + m_{Z'}^2\Gamma_{Z'}^2} \times (85x_H^4 + 152x_H^3 + 104x_H^2 + 32x_H + 4),$$
$$\hat{\sigma}(\bar{d}d \to Z' \to \ell^+\ell^-) = \frac{\pi\alpha_{g_X}^2}{81}\frac{M_{\ell\ell}^2}{(M_{\ell\ell}^2 - m_{Z'}^2)^2 + m_{Z'}^2\Gamma_{Z'}^2} \times (25x_H^4 + 20x_H^3 + 8x_H^2 + 8x_H + 4), \quad (4.2)$$

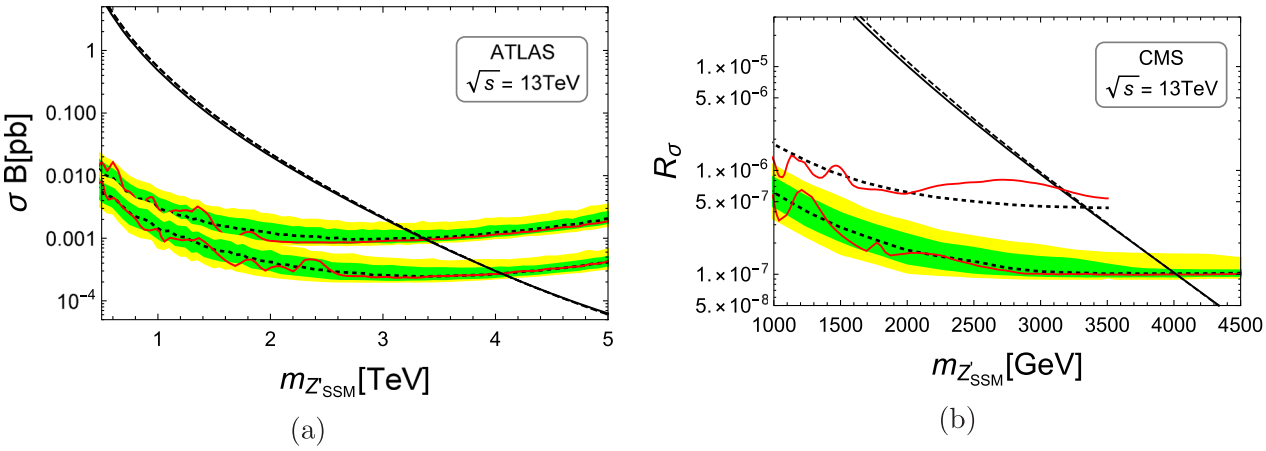

FIG. 3. (a) The cross section as a function of the Z'_{SSM} mass (solid line) with $k = 1.16$, along with the LHC Run-2 ATLAS result from the combined dielectron and dimuon channels in Ref. [95]. (Here we have also shown the ATLAS 2015 result [56] for comparison.) (b) The cross section ratio as a function of the Z'_{SSM} mass (solid line) with $k = 1.42$, along with the LHC Run-2 CMS result from the combined dielectron and dimuon channels in Ref. [96]. (Here we have also shown the CMS 2015 result [57] for comparison.)

where the total decay width of the Z' boson is given in Eq. (3.6). By integrating the differential cross section over a range of $M_{\ell\ell}$ set by the ATLAS and CMS analyses, respectively, we obtain the cross section as a function of x_H, α_{g_X}, and $m_{Z'}$, which are compared with the lower bounds obtained by the ATLAS and CMS collaborations.

In interpreting the ATLAS and the CMS results for the U(1)′ Z' boson, we follow the strategy in Ref. [80]. We first analyze the sequential SM Z' model to check the consistency of our analysis with that of the ATLAS and the CMS collaborations. With the same couplings as the SM, we calculate the differential cross section of the process $pp \to Z'_{SSM} + X \to \ell^+\ell^- + X$ as in Eq. (4.1). According to the analysis by the ATLAS Collaboration at the LHC Run-2, we integrate the differential cross section for the range 120 GeV $\le M_{\ell\ell} \le$ 6000 GeV [95] and obtain the cross section of the dilepton production process as a function of the Z'_{SSM} boson mass. Our result is shown as a solid line in Fig. 3(a), along with the plots presented by the ATLAS Collaboration [95] (Here we also show the ATLAS 2015 result [56] for comparison. We can see that the ATLAS 2016 result has dramatically improved the bound obtained by the ATLAS 2015 result.). In Fig. 3(a), the experimental upper bounds on the Z' boson production cross section are depicted as horizontal solid (red) curves. The theoretical Z' boson production cross section presented in Ref. [95] is shown as the diagonal dashed line, and the lower limit of the Z'_{SSM} boson mass is found to be 4.05 TeV, which can be read off from the intersection point of the theoretical prediction (diagonal dashed line) and the experimental cross section bound [horizontal lower solid (red) curve]. In order to take into account the difference of the parton distribution functions used in the ATLAS analysis and our analysis, and QCD corrections of the process, we have scaled our resultant cross section by a factor $k = 1.16$ in Fig. 3(a), with which we can obtain the same lower limit of the Z'_{SSM} boson mass as 4.05 TeV. We can see that our result (solid line) in Fig. 3(a) with the factor of $k = 1.16$ is very consistent with the theoretical prediction (diagonal dashed line) presented by the ATLAS Collaboration. We use this factor in the following analysis for the U(1)′ Z' production process, when we interpret the ATLAS 2016 result.

We apply the same strategy and compare our results for the Z'_{SSM} model with those in the CMS 2016 results [96]. According to the analysis by the CMS Collaboration, we integrate the differential cross section for the range $0.95m_{Z'_{SSM}} \le M_{\ell\ell} \le 1.05m_{Z'_{SSM}}$ [96] and obtain the cross section. In the CMS analysis, the limits were set on the ratio of the Z'_{SSM} boson cross section to the Z/γ^* cross section:

$$R_\sigma = \frac{\sigma(pp \to Z' + X \to \ell\ell + X)}{\sigma(pp \to Z + X \to \ell\ell + X)}, \tag{4.3}$$

where the Z/γ^* production cross sections in the mass window 60 GeV $\le M_{\ell\ell} \le$ 120 GeV were predicted to be 1928 pb at the LHC Run-2 [96]. Our result for the Z'_{SSM} model is shown as the solid line in Fig. 3(b), along with the plot presented in Ref. [96]. (Here we also show the CMS 2015 result [57] for comparison. We can see that the CMS 2016 result has dramatically improved the bound obtained by the CMS 2015 result.) The analyses in the CMS paper lead to a lower limit of the Z'_{SSM} boson mass of 4.0 TeV, which is read off from the intersection point of the theoretical prediction (diagonal dashed line) and the experimental cross section bound [horizontal lower solid (red) curve]. In order to obtain the same lower mass limits, we have scaled our resultant cross section by a factor $k = 1.42$ in Fig. 3(b). With this k factor, our result (solid line) is very consistent with the theoretical prediction (diagonal dashed

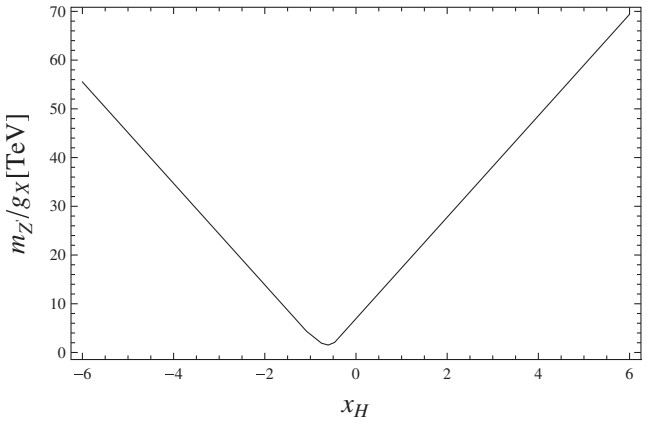

FIG. 4. The lower bound on $m_{Z'}/g_X$ as a function of x_H, obtained by the limits from the final LEP 2 data [99] at the 95% confidence level.

line) presented in Ref. [96]. We use this k factor in our analysis to interpret the CMS result for the U(1)′ Z' boson case.

The search for effective four-Fermi interactions mediated by the Z' boson at LEP leads to a lower bound on $m_{Z'}/g_X$ [97–99]. Employing the limits from the final LEP 2 data [99] at 95% confidence level, we follow Ref. [98] and derive a lower bound on $m_{Z'}/g_X$ as a function x_H. Our result is shown in Fig. 4.

V. COMBINED RESULTS

Now let us combine all of the constraints that we have obtained in the previous sections from the RHN DM physics, collider phenomenology, and the electroweak vacuum stability. In Fig. 5, we show the allowed region in the ($m_{Z'}$, α_{g_X}) plane for fixed $x_H = -0.575$, as an example. The shaded region indicates the parameter space that solves for the electroweak vacuum instability. The (blue) right solid line shows the lower bound on α_{g_X} as a function of $m_{Z'}$ to reproduce the observed DM relic density of the Planck result [94]. The (red) left solid (dashed) line shows the upper bound on α_{g_X} obtained from the search results for the Z' boson resonance by the CMS [96] (ATLAS [95]) Collaboration. The (green) shaded region in between the two solid lines satisfies all constraints. These three constraints work together to narrow the allowed region to be $4\,\text{TeV} \lesssim m_{Z'} \lesssim 8\,\text{TeV}$ and $0.009 \lesssim \alpha_{g_X} \lesssim 0.017$. We also show the naturalness bounds for 10% (right dotted line) and 30% (left dotted line) fine-tuning levels.

In Fig. 6, we show the allowed parameter regions in the (x_H, α_{g_X}) plane for various $m_{Z'}$ values. Figure 6(a) is for $m_{Z'} = 4$ TeV. The shaded region indicates the parameter space that solves the electroweak vacuum instability. The (blue) convex-downward solid line shows the lower bound on α_{g_X} as a function of x_H to reproduce the observed DM relic density. The (red) convex-upward solid (dashed) line shows the upper bound on α_{g_X} obtained from the search

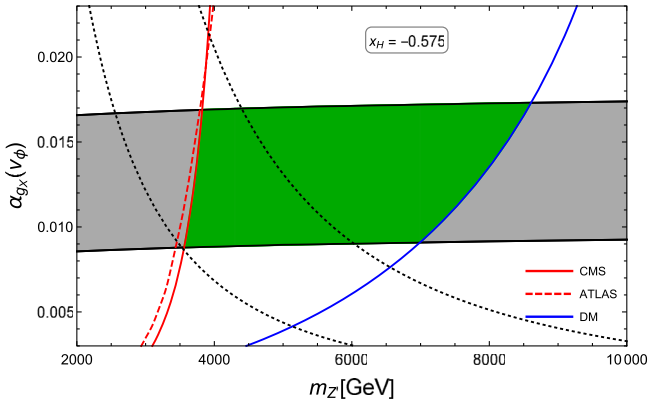

FIG. 5. The allowed regions to solve the electroweak instability problem for $m_{Z'}$ and α_{g_X} with a fixed $x_H = -0.575$ at the TeV scale, along with the dark matter lower bound [(blue) right solid line] on α_{g_X}, the LHC Run-2 (2016) CMS upper bound [(red) solid line] on α_{g_X}, and the LHC Run-2 ATLAS (2016) upper bound [(red) dashed line] on α_{g_X} from direct searches for the Z' boson resonance. The (green) shaded region in between the two solid lines satisfies all constraints. Here, the naturalness bounds for 10% (right dotted line) and 30% (left dotted line) fine-tuning levels are also depicted.

results for the Z' boson resonance by the CMS [96] (ATLAS [95]) Collaboration, and the (red) dashed-dotted lines also show the LEP bounds. The (green) shaded region in between the two solid lines satisfies all constraints. These three constraints work together to narrow the allowed region to be $-1.1 \lesssim x_H \lesssim -0.4$ and $0.002 \lesssim \alpha_{g_X} \lesssim 0.02$. We also show the naturalness bounds for 10% (dashed line) and 30% (dotted line) fine-tuning levels. Figures 6(b), 6(c), and 6(d) are the same as Fig. 6(a), but with $m_{Z'} = 3.75$, 3.5, and 3 TeV, respectively. From Fig. 6(b), the allowed region to satisfy these three constraints indicates $-0.9 \lesssim x_H \lesssim -0.5$ and $0.003 \lesssim \alpha_{g_X} \lesssim 0.015$ for fixed $m_{Z'} = 3.75$ TeV. As $m_{Z'}$ decreases, the LHC upper bound lines are shifted downward, while the DM lower bound line remains almost the same (it moves slightly downward). Therefore, the allowed region between the LHC upper bounds and the DM lower bound narrows. On the other hand, the shaded region remains almost the same, so that the (green) shaded region disappears for $m_{Z'} \lesssim 3.5$ TeV.

VI. DIRECT DETECTION OF RHN DM

A variety of experiments are underway and also planned for directly detecting a DM particle through its elastic scattering off nuclei.[4] In this section, we calculate

[4]We can also consider an indirect detection of the RHN DM through cosmic rays from a pair annihilation of the RHN DM. However, using the parameters in the allowed regions shown in Sec. V, we have found that the pair annihilation cross section is much smaller than the current upper bounds obtained from, for example, the Fermi-LAT experiments [108].

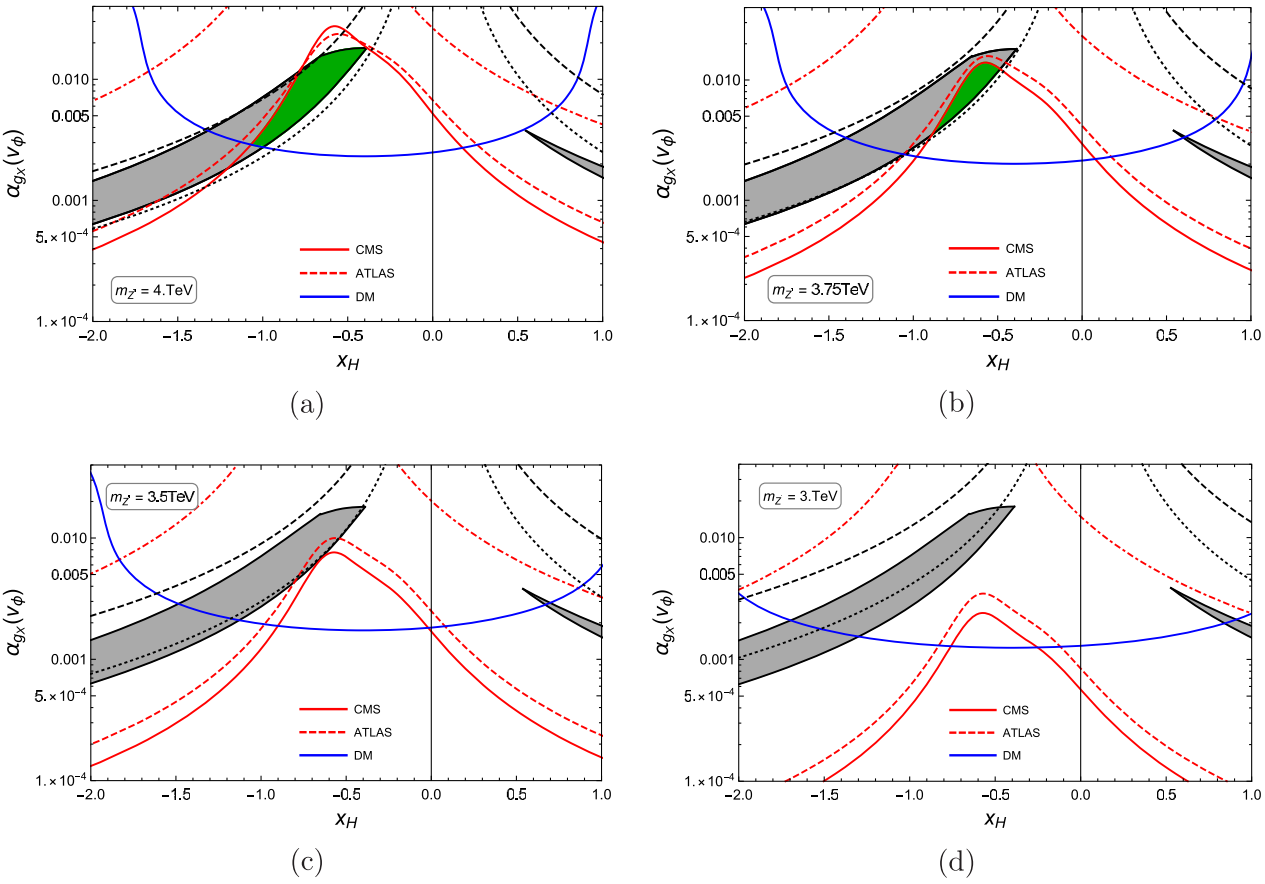

FIG. 6. Allowed parameter regions in the (x_H, α_{g_X}) plane for various $m_{Z'}$ values. Panel (a) is for $m_{Z'} = 4$ TeV. The shaded region indicates the parameter space that solves the electroweak vacuum instability. The (blue) convex-downward solid line shows the cosmological lower bound on α_{g_X} as a function of x_H. The (red) convex-upward solid (dashed) line shows the upper bound on α_{g_X} obtained from the Z' boson search by the CMS [96] (ATLAS [95]) Collaboration, and the (red) dashed-dotted lines show the LEP bounds. The (green) shaded region in between the two solid lines satisfies all constraints. Here, the naturalness bounds for 10% (dashed line) and 30% (dotted line) fine-tuning levels are also depicted. Panels (b), (c), and (d) are the same as panel (a), but with $m_{Z'} = 3.75$, 3.5, and 3 TeV, respectively.

the spin-independent elastic scattering cross section of the RHN DM particle via Higgs-boson exchange,[5] and compare our results with the current experimental results and the prospective reach of future experiments.

From Eq. (2.8), the U(1)′ Higgs VEV v_ϕ is expressed as a function of $m_{Z'}$, α_{g_X}, and x_H:

$$v_\phi^2 = \frac{m_{Z'}^2}{16\pi\alpha_{g_X}}\left[1 - 4\pi\alpha_{g_X}\left(\frac{x_H v_h}{m_{Z'}}\right)^2\right] \simeq \frac{m_{Z'}^2}{16\pi\alpha_{g_X}}. \quad (6.1)$$

[5]There is another process where the RHN DM scatters off nuclei via Z'-boson exchange. Since the RHN DM is a Majorana particle, it only has spin-dependent interaction with nuclei. We have calculated this spin-dependent cross section to be $\sigma_{\rm SD} \sim 10^{-9}$ pb, which is far below the current upper bounds $\sigma_{\rm SD} \lesssim 10^{-4}$ pb obtained from the LUX [109] and IceCube [110] experiments.

In Sec. III, we have also shown that $m_{\rm DM} \simeq m_{Z'}/2$ to satisfy the experimental relic density of the Z'-portal RHN DM, which means $y_{\rm DM} \simeq m_{Z'}/2\sqrt{2}v_\phi \simeq \sqrt{2\pi\alpha_{g_X}}$. Then, Eq. (2.9) is approximately expressed as

$$m_\phi^2 \simeq \frac{1}{8\pi^2}\frac{23}{8}\frac{m_{Z'}^4}{v_\phi^2} \simeq \frac{23}{4\pi}\alpha_{g_X} m_{Z'}^2. \quad (6.2)$$

Using the SM Higgs boson mass in Eq. (2.11), the scalar mass matrix is found to be

$$\mathcal{M} = \begin{pmatrix} m_h^2 & -m_h^2\left(\frac{v_h}{v_\phi}\right) \\ -m_h^2\left(\frac{v_h}{v_\phi}\right) & m_\phi^2 \end{pmatrix}. \quad (6.3)$$

The mass eigenstates h' and ϕ' are defined as

$$\begin{pmatrix} h' \\ \phi' \end{pmatrix} = \begin{pmatrix} \cos\theta & -\sin\theta \\ \sin\theta & \cos\theta \end{pmatrix} \begin{pmatrix} h \\ \phi \end{pmatrix}, \tag{6.4}$$

with the mixing angle θ given by

$$\tan 2\theta = \frac{2m_h^2(v_h/v_\phi)}{m_h^2 - m_\phi^2}, \tag{6.5}$$

and their mass eigenvalues are given by

$$\begin{aligned} m_{h'}^2 &= m_h^2\cos^2\theta + m_\phi^2\sin^2\theta + 2m_h^2\frac{v_h}{v_\phi}\sin\theta\cos\theta \simeq m_h^2, \\ m_{\phi'}^2 &= m_h^2\sin^2\theta + m_\phi^2\cos^2\theta - 2m_h^2\frac{v_h}{v_\phi}\sin\theta\cos\theta \simeq m_\phi^2. \end{aligned} \tag{6.6}$$

Here, we have used the fact that (except for the special case $m_h^2 \simeq m_\phi^2$) the mixing angle is always small because of the suppression by v_h/v_ϕ, with $v_h = 246$ GeV and $v_\phi \gtrsim 10$ TeV. Thus, the mass eigenstate h' is the SM-like Higgs boson, while ϕ' is the U(1)′-like Higgs boson.

The spin-independent elastic scattering cross section with a nucleon is given by

$$\begin{aligned} \sigma_{\rm SI} &= \frac{1}{\pi}(\sqrt{2}y_{\rm DM}\sin\theta\cos\theta)^2\left(\frac{\mu_{\rm DM,N}}{v_h}\right)^2 f_N^2\left(\frac{1}{m_{h'}^2} - \frac{1}{m_{\phi'}^2}\right)^2 \\ &\simeq 4\theta^2\alpha_{g_X}\left(\frac{\mu_{\rm DM,N}}{v_h}\right)^2 f_N^2\left(\frac{1}{m_h^2} - \frac{1}{m_\phi^2}\right)^2, \end{aligned} \tag{6.7}$$

where $\mu_{\rm DM,N} = m_N m_{\rm DM}/(m_N + m_{\rm DM})$ is the reduced mass of the RHN DM–nucleon system with the nucleon mass $m_N = 0.939$ GeV, and

$$f_N = \left(\sum_{q=u,d,s} f_{T_q} + \frac{2}{9}f_{TG}\right)m_N \tag{6.8}$$

is the nuclear matrix element accounting for the quark and gluon contents of the nucleon. In evaluating f_{T_q}, we use the results from lattice QCD simulations [111]: $f_{T_u} + f_{T_d} \simeq 0.056$ and $|f_{T_s}| \le 0.08$. For our conservative analysis, we take $f_{T_s} = 0$ in the following. Using the trace anomaly formula $\sum_{q=u,d,s} f_{T_q} + f_{TG} = 1$ [112–116], we obtain $f_N^2 \simeq 0.0706 m_N^2$. Using Eqs. (6.1), (6.2), and (6.5), $\sigma_{\rm SI}$ is expressed as a function of only two free parameters: α_{g_X} and $m_{Z'}$.

For a fixed $x_H = -0.575$, the resultant spin-independent cross section $\sigma_{\rm SI}$ as a function of $m_{Z'}$ is depicted in Fig. 7. Here, for a fixed $m_{Z'}$ value, α_{g_X} is taken from the shaded region in Fig. 5 to solve the electroweak vacuum instability problem. The (green) shaded region in between around 3.5 and 9 TeV corresponds to the (green) shaded parameter region in Fig. 5, which satisfies all three constraints: the electroweak vacuum stability condition, the LHC Run-2 bound, and the cosmological constraint from the observed RHN DM relic density. The (red) upper solid (dashed) line shows the XENON1T [117] (LUX 2016 [118]) upper bound on $\sigma_{\rm SI}$ as a function of $m_{Z'} \simeq 2m_{\rm DM}$, and the (red) dotted line shows the prospective reach for the upper bound on $\sigma_{\rm SI}$ in the next-generation successor of the LUX experiment, the LUX-ZEPLIN (LZ) DM experiment [119].

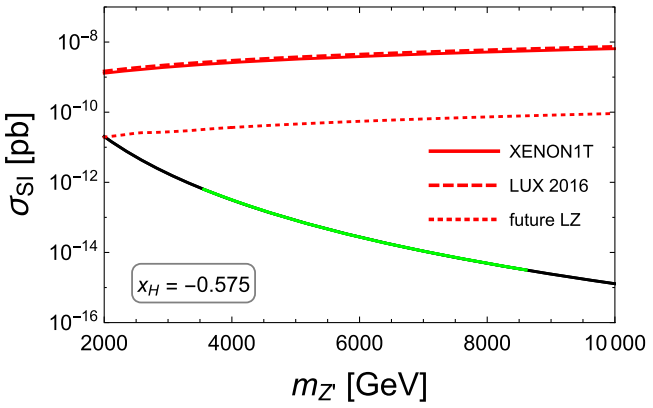

FIG. 7. The resultant spin-independent cross section $\sigma_{\rm SI}$ as a function of $m_{Z'}$ for a fixed $x_H = -0.575$. Here, for a fixed $m_{Z'}$ value, α_{g_X} is taken from the shaded region in Fig. 5 to solve the electroweak vacuum instability problem. The (green) shaded region between around 3.5 and 9 TeV corresponds to the (green) shaded parameter region in Fig. 5, which satisfies all three constraints: the electroweak vacuum stability condition, the LHC Run-2 bound, and the cosmological constraint from the observed RHN DM relic density. The (red) upper solid (dashed) line shows the XENON1T [117] (LUX 2016 [118]) upper bound on $\sigma_{\rm SI}$ as a function of $m_{Z'} \simeq 2m_{\rm DM}$, and the (red) dotted line shows the prospective reach for the upper bound on $\sigma_{\rm SI}$ in the next-generation successor of the LUX experiment, the LUX-ZEPLIN (LZ) DM experiment [119].

In Fig. 8, we show the resultant $\sigma_{\rm SI}$ in the $(x_H, \sigma_{\rm SI})$ plane for various $m_{Z'}$ values, corresponding to the parameter regions shown in Fig. 6. Figure 8(a) shows our results for $m_{Z'} = 4$ TeV. The shaded regions indicate the parameter space that solves the electroweak vacuum instability. The (green) shaded region in the range $-1.1 \lesssim x_H \lesssim -0.4$ corresponds to the (green) shaded region in Fig. 6(a), which satisfies all three constraints: the electroweak vacuum stability condition, the LHC Run-2 bound, and the cosmological constraint from the observed RHN DM relic density. The (red) upper solid (dashed) line shows the XENON1T [117] (LUX 2016 [118]) upper bound on $\sigma_{\rm SI}$, and the (red) dotted line shows the prospective reach for the upper bound on $\sigma_{\rm SI}$ in the LZ DM experiment [119]. Figures 8(b), 8(c), and 8(d) are the same as Fig. 8(a), but for $m_{Z'} = 3.75$, 3.5, and 3 TeV, corresponding to Figs. 6(b), 6(c), and 6(d), respectively. Figure 8(b) has a (green) shaded region in the range $-0.9 \lesssim x_H \lesssim -0.5$ to satisfy

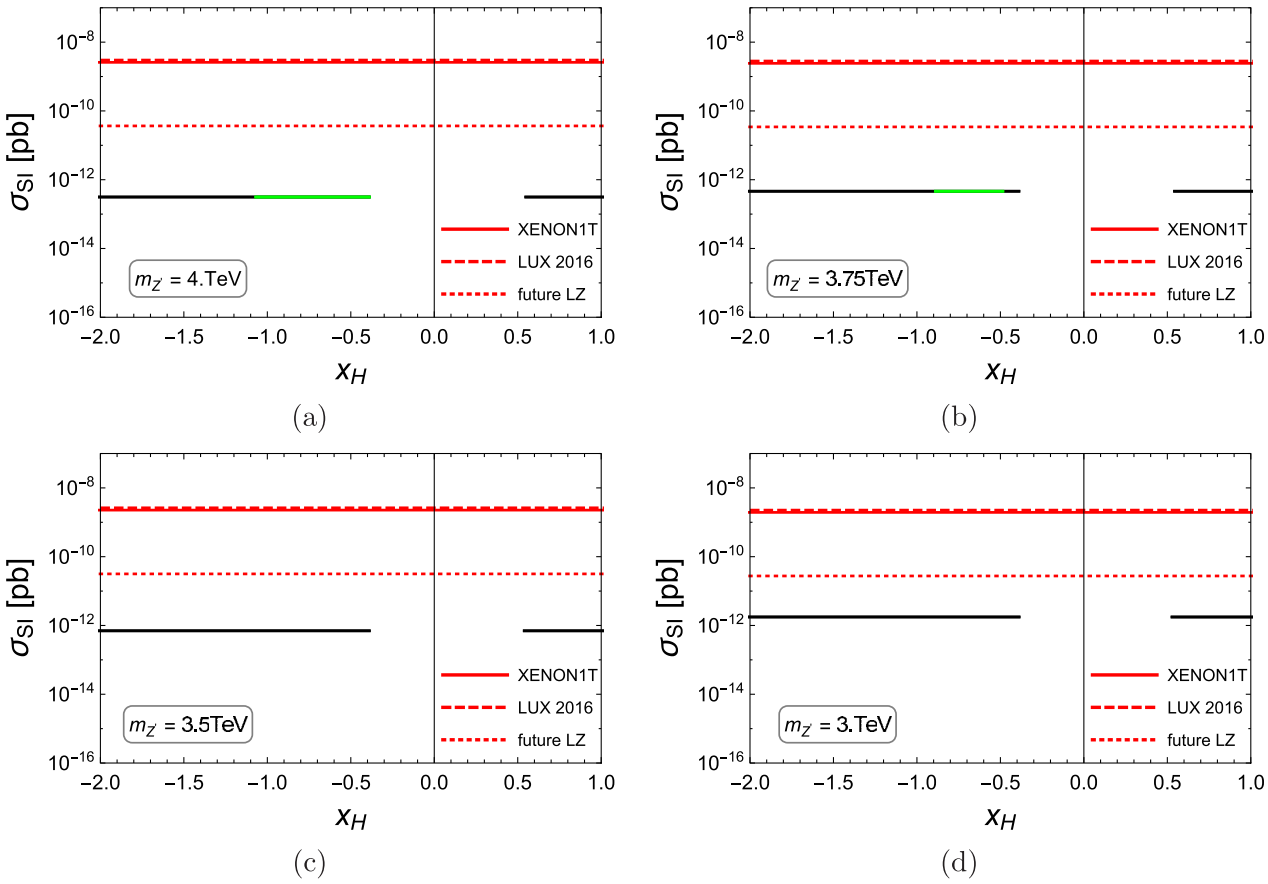

FIG. 8. The resultant σ_{SI} in the (x_H, σ_{SI}) plane for various $m_{Z'}$ values, corresponding to the parameter regions shown in Fig. 6. Panel (a) shows our results for $m_{Z'} = 4$ TeV. The shaded regions indicate the parameter space that solves the electroweak vacuum instability. The (green) shaded region in the range $-1.1 \lesssim x_H \lesssim -0.4$ corresponds to the (green) shaded region in Fig. 6(a), which satisfies all three constraints: the electroweak vacuum stability condition, the LHC Run-2 bound, and the cosmological constraint from the observed RHN DM relic density. The (red) upper solid (dashed) line shows the XENON1T [117] (LUX 2016 [118]) upper bound on σ_{SI}, and the (red) dotted line shows the prospective reach for the upper bound on σ_{SI} in the LZ DM experiment [119]. Panels (b), (c), and (d) are the same as panel (a), but with $m_{Z'} = 3.75$, 3.5, and 3 TeV, corresponding to Figs. 6(b), 6(c), and 6(d), respectively.

the three constraints, while Figs. 8(c) and 8(d) have no such region.

VII. CONCLUSIONS

We have considered the DM scenario in the context of the classically conformal U(1)′ extended SM, with three RHNs and the U(1)′ Higgs field. The model is free from all of the U(1)′ gauge and gravitational anomalies in the presence of the three RHNs. We have introduced a Z_2 parity in the model, under which an odd parity is assigned to one RHN, while all of the other particles are assigned to be Z_2 even. In our model, the Z_2-odd RHN serves as a stable DM candidate, while the other two RHNs are utilized for the minimal seesaw mechanism in order to reproduce the neutrino oscillation data and the observed baryon asymmetry of the Universe through leptogenesis. In this model, the U(1)′ gauge symmetry is radiatively broken through the CW mechanism, by which the electroweak symmetry breaking is triggered. There are three free parameters in our model: the U(1)′ charge of the SM Higgs doublet (x_H), the new U(1)′ gauge coupling (α_{g_X}), and the U(1)′ gauge boson (Z') mass ($m_{Z'}$).

In this model context, we first investigated the possibility of resolving the electroweak vacuum instability with the current world average of the experimental data, $m_t = 173.34$ GeV and $m_h = 125.09$ GeV. By analyzing the RG evolutions of the couplings of the model at the two-loop level, we performed a parameter scan for the three parameters $m_{Z'}$, α_{g_X} and x_H, and identified parameter regions which can solve the electroweak instability problem and keep all coupling values in the perturbative regime up to the Planck mass scale. We found that the resultant parameter regions are very severely constrained. Next, we calculated the thermal relic density of the RHN DM and identified the model parameter region to reproduce the observed DM relic density of the Planck 2015 measurement. In our model, the RHN DM particles mainly

annihilate into the SM particles through the s-channel process mediated by the Z' boson. We obtained the lower bound on α_{g_X} as a function of $m_{Z'}$ and x_H from the observed DM relic density. We also considered the LHC Run-2 bounds from the search for the Z' boson resonance by the recent ATLAS and CMS analysis, which lead to the upper bounds on α_{g_X} as a function of $m_{Z'}$ and x_H. The LEP results from the search for effective four-Fermi interactions mediated by the Z' boson can also constrain the model parameter space, but the LEP constraints are found to be weaker than those obtained from the LHC Run-2 results. Finally, we combined all of the constraints. The cosmological constraint on the RHN DM yields the lower bound on α_{g_X} as a function of $m_{Z'}$ and x_H, while the upper bound on α_{g_X} is obtained from the LHC Run-2 results, so that these constraints work together to narrow the allowed parameter regions. We found that only small portions of these allowed parameter regions can solve the electroweak vacuum instability problem. In particular, there is no allowed region that satisfies all constraints for $m_{Z'} \lesssim 3.5$ TeV. For the obtained allowed regions, we calculated the spin-independent cross section of the RHN DM with nucleons. We found that the resultant cross section is well below the current experimental upper bounds.

ACKNOWLEDGMENTS

The work of D.-s.T. and S.O. is supported by the Advanced Medical Instrumentation unit [Sugawara unit] and Mathematical and Theoretical Physics unit [Hikami unit], respectively, of the Okinawa Institute of Science and Technology Graduate University. The work of N.O. is supported in part by the United States Department of Energy (DE-SC0013680).

[1] P. Minkowski, $\mu \to e\gamma$ at a rate of one out of 10^9 muon decays?, Phys. Lett. B **67**, 421 (1977).
[2] T. Yanagida, Horizontal symmetry and masses of neutrinos, *Conf. Proc.*, C7902131, 95 (1979).
[3] M. Gell-Mann, P. Ramond, and R. Slansky, Complex spinors and unified theories, *Conf. Proc.*, C790927, 315 (1979).
[4] S. L. Glashow, The future of elementary particle physics, *NATO Sci. Ser. B* 61, 687 (1980).
[5] R. N. Mohapatra and G. Senjanovic, Neutrino Mass and Spontaneous Parity Nonconservation, Phys. Rev. Lett. **44**, 912 (1980).
[6] R. N. Mohapatra and R. E. Marshak, Local $B - L$ Symmetry of Electroweak Interactions, Majorana Neutrinos and Neutron Oscillations, Phys. Rev. Lett. **44**, 1316 (1980); Erratum, Phys. Rev. Lett. **44**, 1644 (1980).
[7] R. E. Marshak and R. N. Mohapatra, Quark-lepton symmetry and $B - L$ as the U(1) generator of the electroweak symmetry group, Phys. Lett. B **91**, 222 (1980).
[8] C. Wetterich, Neutrino masses and the scale of $B - L$ violation, Nucl. Phys. **B187**, 343 (1981).
[9] A. Masiero, J. F. Nieves, and T. Yanagida, $B - L$ violating proton decay and late cosmological baryon production, Phys. Lett. B **116**, 11 (1982).
[10] R. N. Mohapatra and G. Senjanovic, Spontaneous breaking of global $B - L$ symmetry and matter-antimatter oscillations in grand unified theories, Phys. Rev. D **27**, 254 (1983).
[11] W. Buchmuller, C. Greub, and P. Minkowski, Neutrino masses, neutral vector bosons and the scale of $B - L$ breaking, Phys. Lett. B **267**, 395 (1991).
[12] T. Appelquist, B. A. Dobrescu, and A. R. Hopper, Nonexotic neutral gauge bosons, Phys. Rev. D **68**, 035012 (2003).
[13] S. Oda, N. Okada, and D.-s. Takahashi, Classically conformal U(1)′ extended standard model and Higgs vacuum stability, Phys. Rev. D **92**, 015026 (2015).
[14] A. Das, S. Oda, N. Okada, and D.-s. Takahashi, Classically conformal U(1)′ extended standard model, electroweak vacuum stability, and LHC Run-2 bounds, Phys. Rev. D **93**, 115038 (2016).
[15] R. Hempfling, The next-to-minimal Coleman-Weinberg model, Phys. Lett. B **379**, 153 (1996).
[16] A. G. Dias, Neutrino mass through concomitant breakdown of the U(1) chiral and scale symmetries, Phys. Rev. D **73**, 096002 (2006).
[17] J. R. Espinosa and M. Quiros, Novel effects in electroweak breaking from a hidden sector, Phys. Rev. D **76**, 076004 (2007).
[18] W.-F. Chang, J. N. Ng, and J. M. S. Wu, Shadow Higgs boson from a scale-invariant hidden $U(1)_s$ model, Phys. Rev. D **75**, 115016 (2007).
[19] R. Foot, A. Kobakhidze, and R. R. Volkas, Electroweak Higgs as a pseudo-Goldstone boson of broken scale invariance, Phys. Lett. B **655**, 156 (2007).
[20] R. Foot, A. Kobakhidze, K. McDonald, and R. Volkas, Neutrino mass in radiatively-broken scale-invariant models, Phys. Rev. D **76**, 075014 (2007).
[21] K. A. Meissner and H. Nicolai, Conformal symmetry and the Standard Model, Phys. Lett. B **648**, 312 (2007).
[22] R. Foot, A. Kobakhidze, K. L. McDonald, and R. R. Volkas, Solution to the hierarchy problem from an almost decoupled hidden sector within a classically scale invariant theory, Phys. Rev. D **77**, 035006 (2008).
[23] K. A. Meissner and H. Nicolai, Effective action, conformal anomaly and the issue of quadratic divergences, Phys. Lett. B **660**, 260 (2008).
[24] K. A. Meissner and H. Nicolai, Neutrinos, axions and conformal symmetry, Eur. Phys. J. C **57**, 493 (2008).
[25] S. Iso, N. Okada, and Y. Orikasa, Classically conformal $B - L$ extended Standard Model, Phys. Lett. B **676**, 81 (2009).

[26] S. Iso, N. Okada, and Y. Orikasa, Minimal $B-L$ model naturally realized at TeV scale, Phys. Rev. D **80**, 115007 (2009).
[27] M. Holthausen, M. Lindner, and M. A. Schmidt, Radiative symmetry breaking of the minimal left-right symmetric model, Phys. Rev. D **82**, 055002 (2010).
[28] A. Farzinnia, H.-J. He, and J. Ren, Natural electroweak symmetry breaking from scale invariant Higgs mechanism, Phys. Lett. B **727**, 141 (2013).
[29] M. Heikinheimo, A. Racioppi, M. Raidal, C. Spethmann, and K. Tuominen, Physical naturalness and dynamical breaking of classical scale invariance, Mod. Phys. Lett. A **29**, 1450077 (2014).
[30] A. Farzinnia and J. Ren, Higgs partner searches and dark matter phenomenology in a classically scale invariant Higgs boson sector, Phys. Rev. D **90**, 015019 (2014).
[31] M. Lindner, S. Schmidt, and J. Smirnov, Neutrino masses and conformal electro-weak symmetry breaking, J. High Energy Phys. 10 (2014) 177.
[32] V. V. Khoze, C. McCabe, and G. Ro, Higgs vacuum stability from the dark matter portal, J. High Energy Phys. 08 (2014) 026.
[33] E. Gabrielli, M. Heikinheimo, K. Kannike, A. Racioppi, M. Raidal, and C. Spethmann, Towards completing the Standard Model: Vacuum stability, electroweak symmetry breaking, and dark matter, Phys. Rev. D **89**, 015017 (2014).
[34] W. Altmannshofer, W. A. Bardeen, M. Bauer, M. Carena, and J. D. Lykken, Light dark matter, naturalness, and the radiative origin of the electroweak scale, J. High Energy Phys. 01 (2015) 032.
[35] A. Karam and K. Tamvakis, Dark matter and neutrino masses from a scale-invariant multi-Higgs portal, Phys. Rev. D **92**, 075010 (2015).
[36] N. Haba, H. Ishida, N. Okada, and Y. Yamaguchi, Electroweak symmetry breaking through bosonic seesaw mechanism in a classically conformal extension of the Standard Model, arXiv:1509.01923.
[37] H. Okada, Y. Orikasa, and K. Yagyu, Higgs triplet model with classically conformal invariance, arXiv:1510.00799.
[38] A. Latosinski, A. Lewandowski, K. A. Meissner, and H. Nicolai, Conformal Standard Model with an extended scalar sector, J. High Energy Phys. 10 (2015) 170.
[39] Z.-W. Wang, F. S. Sage, T. G. Steele, and R. B. Mann, Asymptotic safety in the conformal hidden sector?, arXiv:1511.02531.
[40] F. Goertz, Electroweak symmetry breaking without the μ^2 term, Phys. Rev. D **94**, 015013 (2016).
[41] N. Haba, H. Ishida, N. Okada, and Y. Yamaguchi, Bosonic seesaw mechanism in a classically conformal extension of the Standard Model, Phys. Lett. B **754**, 349 (2016).
[42] N. Haba, H. Ishida, R. Takahashi, and Y. Yamaguchi, Gauge coupling unification in a classically scale invariant model, J. High Energy Phys. 02 (2016) 058.
[43] K. Ghorbani and H. Ghorbani, Scalar dark matter in scale invariant Standard Model, J. High Energy Phys. 04 (2016) 024.
[44] N. Haba, H. Ishida, N. Kitazawa, and Y. Yamaguchi, A new dynamics of electroweak symmetry breaking with classically scale invariance, Phys. Lett. B **755**, 439 (2016).
[45] A. Ahriche, K. L. McDonald, and S. Nasri, A radiative model for the weak scale and neutrino mass via dark matter, J. High Energy Phys. 02 (2016) 038.
[46] H. Ishida, S. Matsuzaki, and Y. Yamaguchi, Invisible axionlike dark matter from the electroweak bosonic seesaw mechanism, Phys. Rev. D **94**, 095011 (2016).
[47] H. Hatanaka, D.-W. Jung, and P. Ko, AdS/QCD approach to the scale-invariant extension of the standard model with a strongly interacting hidden sector, J. High Energy Phys. 08 (2016) 094.
[48] A. Karam and K. Tamvakis, Dark matter from a classically scale-invariant $SU(3)_X$, Phys. Rev. D **94**, 055004 (2016).
[49] L. Marzola and A. Racioppi, Minimal but non-minimal inflation and electroweak symmetry breaking, J. Cosmol. Astropart. Phys. 10 (2016) 010.
[50] A. Das, N. Okada, and N. Papapietro, Electroweak vacuum stability in classically conformal $B-L$ extension of the Standard Model, Eur. Phys. J. C **77**, 122 (2017).
[51] K. Kannike, M. Raidal, C. Spethmann, and H. Veermäe, The evolving Planck mass in classically scale-invariant theories, J. High Energy Phys. 04 (2017) 026.
[52] L. Marzola, A. Racioppi, and V. Vaskonen, Phase transition and gravitational wave phenomenology of scalar conformal extensions of the Standard Model, Eur. Phys. J. C **77**, 484 (2017).
[53] S. R. Coleman and E. J. Weinberg, Radiative corrections as the origin of spontaneous symmetry breaking, Phys. Rev. D **7**, 1888 (1973).
[54] ATLAS, CDF, CMS, and D0 Collaborations, First combination of Tevatron and LHC measurements of the top-quark mass, arXiv:1403.4427.
[55] G. Aad *et al.* (ATLAS and CMS Collaborations), Combined Measurement of the Higgs Boson Mass in pp Collisions at $\sqrt{s}=7$ and 8 TeV with the ATLAS and CMS Experiments, Phys. Rev. Lett. **114**, 191803 (2015).
[56] ATLAS Collaboration, Search for new phenomena in the dilepton final state using proton-proton collisions at $\sqrt{s}=13$ TeV with the ATLAS detector, Report No. ATLAS-CONF-2015-070.
[57] CMS Collaboration, Search for a narrow resonance produced in 13 TeV pp collisions decaying to electron pair or muon pair final states, Report No. CMS-PAS-EXO-15-005.
[58] N. Okada and O. Seto, Higgs portal dark matter in the minimal gauged $U(1)_{B-L}$ model, Phys. Rev. D **82**, 023507 (2010).
[59] A. Anisimov and P. Di Bari, Cold dark matter from heavy right-handed neutrino mixing, Phys. Rev. D **80**, 073017 (2009).
[60] M. Fukugita and T. Yanagida, Baryogenesis without grand unification, Phys. Lett. B **174**, 45 (1986).
[61] S. F. King, Large mixing angle MSW and atmospheric neutrinos from single right-handed neutrino dominance and U(1) family symmetry, Nucl. Phys. **B576**, 85 (2000).
[62] P. H. Frampton, S. L. Glashow, and T. Yanagida, Cosmological sign of neutrino CP violation, Phys. Lett. B **548**, 119 (2002).

[63] Z. M. Burell and N. Okada, Supersymmetric minimal $B-L$ model at the TeV scale with right-handed Majorana neutrino dark matter, Phys. Rev. D **85**, 055011 (2012).
[64] L. Basso, O. Fischer, and J. J. van der Bij, Natural Z' model with an inverse seesaw mechanism and leptonic dark matter, Phys. Rev. D **87**, 035015 (2013).
[65] E. Dudas, L. Heurtier, Y. Mambrini, and B. Zaldivar, Extra U(1), effective operators, anomalies and dark matter, J. High Energy Phys. 11 (2013) 083.
[66] M. Das and S. Mohanty, Leptophilic dark matter in gauged $L_\mu - L_\tau$ extension of MSSM, Phys. Rev. D **89**, 025004 (2014).
[67] X. Chu, Y. Mambrini, J. Quevillon, and B. Zaldivar, Thermal and non-thermal production of dark matter via Z'-portal(s), J. Cosmol. Astropart. Phys. 01 (2014) 034.
[68] M. Lindner, D. Schmidt, and A. Watanabe, Dark matter and $U(1)'$ symmetry for the right-handed neutrinos, Phys. Rev. D **89**, 013007 (2014).
[69] A. Alves, S. Profumo, and F. S. Queiroz, The dark Z' portal: direct, indirect and collider searches, J. High Energy Phys. 04 (2014) 063.
[70] J. Kopp, L. Michaels, and J. Smirnov, Loopy constraints on leptophilic dark matter and internal bremsstrahlung, J. Cosmol. Astropart. Phys. 04 (2014) 022.
[71] P. Agrawal, Z. Chacko, and C. B. Verhaaren, Leptophilic dark matter and the anomalous magnetic moment of the muon, J. High Energy Phys. 08 (2014) 147.
[72] D. Hooper, Z' mediated dark matter models for the Galactic Center gamma-ray excess, Phys. Rev. D **91**, 035025 (2015).
[73] E. Ma and R. Srivastava, Dirac or inverse seesaw neutrino masses with $B-L$ gauge symmetry and S_3 flavor symmetry, Phys. Lett. B **741**, 217 (2015).
[74] A. Alves, A. Berlin, S. Profumo, and F. S. Queiroz, Dark matter complementarity and the Z' portal, Phys. Rev. D **92**, 083004 (2015).
[75] K. Ghorbani and H. Ghorbani, Two-portal dark matter, Phys. Rev. D **91**, 123541 (2015).
[76] B. L. Sánchez-Vega and E. R. Schmitz, Fermionic dark matter and neutrino masses in a $B-L$ model, Phys. Rev. D **92**, 053007 (2015).
[77] M. Duerr, P. Fileviez Perez, and J. Smirnov, Simplified Dirac dark matter models and gamma-ray lines, Phys. Rev. D **92**, 083521 (2015).
[78] A. Alves, A. Berlin, S. Profumo, and F. S. Queiroz, Dirac-fermionic dark matter in $U(1)_X$ models, J. High Energy Phys. 10 (2015) 076.
[79] E. Ma, N. Pollard, R. Srivastava, and M. Zakeri, Gauge $B-L$ model with residual Z_3 symmetry, Phys. Lett. B **750**, 135 (2015).
[80] N. Okada and S. Okada, Z'_{BL} portal dark matter and LHC Run-2 results, Phys. Rev. D **93**, 075003 (2016).
[81] N. Okada and N. Papapietro, R-parity conserving minimal SUSY $B-L$ model, arXiv:1603.01769.
[82] W. Chao, H.-k. Guo, and Y. Zhang, Majorana dark matter with B + L gauge symmetry, J. High Energy Phys. 04 (2017) 034.
[83] A. Biswas, S. Choubey, and S. Khan, Galactic gamma ray excess and dark matter phenomenology in a $U(1)_{B-L}$ model, J. High Energy Phys. 08 (2016) 114.
[84] E. Accomando, C. Coriano, L. Delle Rose, J. Fiaschi, C. Marzo, and S. Moretti, Z', Higgses and heavy neutrinos in $U(1)'$ models: from the LHC to the GUT scale, J. High Energy Phys. 07 (2016) 086.
[85] M. Fairbairn, J. Heal, F. Kahlhoefer, and P. Tunney, Constraints on Z' models from LHC dijet searches and implications for dark matter, J. High Energy Phys. 09 (2016) 018.
[86] M. Klasen, F. Lyonnet, and F. S. Queiroz, NLO + NLL collider bounds, Dirac fermion and scalar dark matter in the $B-L$ Model, Eur. Phys. J. C **77**, 348 (2017).
[87] P. S. Bhupal Dev, R. N. Mohapatra, and Y. Zhang, Naturally stable right-handed neutrino dark matter, J. High Energy Phys. 11 (2016) 077.
[88] W. Altmannshofer, S. Gori, S. Profumo, and F. S. Queiroz, Explaining dark matter and B decay anomalies with an $L_\mu - L_\tau$ model, J. High Energy Phys. 12 (2016) 106.
[89] N. Okada and S. Okada, Z'-portal right-handed neutrino dark matter in the minimal $U(1)_X$ extended Standard Model, Phys. Rev. D **95**, 035025 (2017).
[90] K. Kaneta, Z. Kang, and H.-S. Lee, Right-handed neutrino dark matter under the $B-L$ gauge interaction, J. High Energy Phys. 02 (2017) 031.
[91] G. Arcadi, M. Dutra, P. Ghosh, M. Lindner, Y. Mambrini, M. Pierre, S. Profumo, and F. S. Queiroz, The waning of the WIMP? A review of models, searches, and constraints, arXiv:1703.07364.
[92] N. Okada and Y. Orikasa, Dark matter in the classically conformal $B-L$ model, Phys. Rev. D **85**, 115006 (2012).
[93] T. Basak and T. Mondal, Constraining minimal $U(1)_{B-L}$ model from dark matter observations, Phys. Rev. D **89**, 063527 (2014).
[94] N. Aghanim *et al.* (Planck Collaboration), Planck 2015 results. XI. CMB power spectra, likelihoods, and robustness of parameters, Astron. Astrophys. **594**, A11 (2016).
[95] ATLAS Collaboration, Search for new high-mass resonances in the dilepton final state using proton-proton collisions at $\sqrt{s} = 13$ TeV with the ATLAS detector, Report No. ATLAS-CONF-2016-045.
[96] CMS Collaboration, Search for a high-mass resonance decaying into a dilepton final state in 13 fb^{-1} of pp collisions at $\sqrt{s} = 13$ TeV, Report No. CMS-PAS-EXO-16-031.
[97] The LEP Collaborations ALEPH, DELPHI, L3, and OPAL, the LEP Electroweak Working Group, the SLD Electroweak and Heavy Flavour Groups, A combination of preliminary electroweak measurements and constraints on the standard model, arXiv:hep-ex/0312023.
[98] M. Carena, A. Daleo, B. A. Dobrescu, and T. M. P. Tait, Z' gauge bosons at the Fermilab Tevatron, Phys. Rev. D **70**, 093009 (2004).
[99] ALEPH, DELPHI, OPAL, and L3 Collaborations, and the LEP Electroweak Working Group, Electroweak measurements in electron-positron collisions at W-boson-pair energies at LEP, Phys. Rep. **532**, 119 (2013).
[100] D. Buttazzo, G. Degrassi, P. P. Giardino, G. F. Giudice, F. Sala, A. Salvio, and A. Strumia, Investigating the near-criticality of the Higgs boson, J. High Energy Phys. 12 (2013) 089.

[101] C. Coriano, L. Delle Rose, and C. Marzo, Vacuum stability in U(1)-prime extensions of the Standard Model with TeV scale right handed neutrinos, Phys. Lett. B **738**, 13 (2014).
[102] S. Di Chiara, V. Keus, and O. Lebedev, Stabilizing the Higgs potential with a Z', Phys. Lett. B **744**, 59 (2015).
[103] C. Coriano, L. Delle Rose, and C. Marzo, Constraints on Abelian extensions of the Standard Model from two-loop vacuum stability and $U(1)_{B-L}$, J. High Energy Phys. 02 (2016) 135.
[104] J. A. Casas, J. R. Espinosa, and I. Hidalgo, Implications for new physics from fine-tuning arguments. 1. Application to SUSY and seesaw cases, J. High Energy Phys. 11 (2004) 057.
[105] N. F. Bell, Y. Cai, and R. K. Leane, Impact of mass generation for spin-1 mediator simplified models, J. Cosmol. Astropart. Phys. 01 (2017) 039.
[106] V. D. Barger, W.-Y. Keung, and E. Ma, Doubling of weak gauge bosons in an extension of the Standard Model, Phys. Rev. Lett. **44**, 1169 (1980).
[107] J. Pumplin, D. R. Stump, J. Huston, H. L. Lai, P. M. Nadolsky, and W. K. Tung, New generation of parton distributions with uncertainties from global QCD analysis, J. High Energy Phys. 07 (2002) 012.
[108] E. Charles *et al.* (Fermi-LAT Collaboration), Sensitivity projections for dark matter searches with the Fermi Large Area Telescope, Phys. Rep. **636**, 1 (2016).
[109] C. F. P. da Silva (LUX Collaboration), Dark matter searches with LUX, arXiv:1710.03572.
[110] M. G. Aartsen *et al.* (IceCube Collaboration), Search for annihilating dark matter in the Sun with 3 years of IceCube data, Eur. Phys. J. C **77**, 146 (2017).
[111] H. Ohki, H. Fukaya, S. Hashimoto, T. Kaneko, H. Matsufuru, J. Noaki, T. Onogi, E. Shintani, and N. Yamada, Nucleon sigma term and strange quark content from lattice QCD with exact chiral symmetry, Phys. Rev. D **78**, 054502 (2008).
[112] R. J. Crewther, Nonperturbative evaluation of the anomalies in low-energy theorems, Phys. Rev. Lett. **28**, 1421 (1972).
[113] M. S. Chanowitz and J. R. Ellis, Canonical anomalies and broken scale invariance, Phys. Lett. B **40**, 397 (1972).
[114] M. S. Chanowitz and J. R. Ellis, Canonical trace anomalies, Phys. Rev. D **7**, 2490 (1973).
[115] J. C. Collins, A. Duncan, and S. D. Joglekar, Trace and dilatation anomalies in gauge theories, Phys. Rev. D **16**, 438 (1977).
[116] M. A. Shifman, A. I. Vainshtein, and V. I. Zakharov, Remarks on Higgs boson interactions with nucleons, Phys. Lett. B **78**, 443 (1978).
[117] E. Aprile *et al.* (XENON Collaboration), First dark matter search results from the XENON1T experiment, Phys. Rev. Lett. **119**, 181301 (2017).
[118] D. S. Akerib *et al.* (LUX Collaboration), Results from a search for dark matter in the complete LUX exposure, Phys. Rev. Lett. **118**, 021303 (2017).
[119] M. Szydagis (LUX and LZ Collaborations), The present and future of searching for dark matter with LUX and LZ, *Proc. Sci.*, ICHEP2016 (2016) 220, arXiv:1611.05525.